ARTICLE

BIOTECHNOLOGY and BIOENGINEERING

Analysis of NADPH Supply During Xylitol Production by Engineered *Escherichia coli*

Jonathan W. Chin,[1] Reza Khankal, Caroline A. Monroe, Costas D. Maranas, Patrick C. Cirino

Department of Chemical Engineering, Pennsylvania State University, University Park, Pennsylvania 16802; telephone: 814-865-5790; fax: 814-865-7846; e-mail: cirino@engr.psu.edu

Received 12 March 2008; revision received 19 June 2008; accepted 24 June 2008

Published online 22 July 2008 in Wiley InterScience (www.interscience.wiley.com). DOI 10.1002/bit.22060

ABSTRACT: *Escherichia coli* strain PC09 (Δ*xylB*, cAMP-independent CRP (*crp**) mutant) expressing an NADPH-dependent xylose reductase from *Candida boidinii* (CbXR) was previously reported to produce xylitol from xylose while metabolizing glucose [Cirino et al. (2006) Biotechnol Bioeng 95(6): 1167–1176]. This study aims to understand the role of NADPH supply in xylitol yield and the contribution of key central carbon metabolism enzymes toward xylitol production. Studies in which the expression of CbXR or a xylose transporter was increased suggest that enzyme activity and xylose transport are not limiting xylitol production in PC09. A constraints-based stoichiometric metabolic network model was used to understand the roles of central carbon metabolism reactions and xylose transport energetics on the theoretical maximum molar xylitol yield (xylitol produced per glucose consumed), and xylitol yields (Y_{RPG}) were measured from resting cell biotransformations with various PC09 derivative strains. For the case of xylose-proton symport, omitting the Zwf (glucose-6-phosphate dehydrogenase) or PntAB (membrane-bound transhydrogenase) reactions or TCA cycle activity from the model reduces the theoretical maximum yield from 9.2 to 8.8, 3.6, and 8.0 mol xylitol (mol glucose)$^{-1}$, respectively. Experimentally, deleting *pgi* (encoding phosphoglucose isomerase) from strain PC09 improves the yield from 3.4 to 4.0 mol xylitol (mol glucose)$^{-1}$, while deleting either or both *E. coli* transhydrogenases (*sthA* and *pntA*) has no significant effect on the measured yield. Deleting either *zwf* or *sucC* (TCA cycle) significantly reduces the yield from 3.4 to 2.0 and 2.3 mol xylitol (mol glucose)$^{-1}$, respectively. Expression of a xylose reductase with relaxed cofactor specificity increases the yield to 4.0. The large discrepancy between theoretical maximum and experimentally determined yield values suggests that biocatalysis is compromised by pathways competing for reducing equivalents and dissipating energy. The metabolic role of transhydrogenases during *E. coli* biocatalysis has remained largely unspecified. Our results demonstrate the importance of direct NADPH supply by $NADP^+$-utilizing enzymes in central metabolism for driving heterologous NADPH-dependent reactions, and suggest that the pool of reduced cofactors available for biotransformation is not readily interchangeable via transhydrogenase.

Biotechnol. Bioeng. 2009;102: 209–220.

KEYWORDS: xylitol; *Escherichia coli*; xylose reductase; biocatalysis; resting cells; transhydrogenase

Introduction

Biotransformations are increasingly popular alternatives to traditional chemical catalysis because of relatively inexpensive feedstocks, unmatched selectivity offered by enzymes, and the potential for clean, green processes. One important class of biotransformations are redox reactions requiring the reduced nicotinamide cofactors NAD(P)H to catalyze oxygen insertion (oxygenases) or reduction of carbonyl groups (reductases or dehydrogenases). Cost-effective, continuous delivery of reduced cofactors remains an important challenge associated with utilizing cofactor-dependent enzymes for biocatalysis. Currently, in vitro cofactor regeneration systems are commonly used, whereby a cosubstrate such as formate or glucose undergoes a single (two electron) oxidation that results in regeneration of a stoichiometric amount of NADH or NADPH (van der Donk and Zhao, 2003). In many scenarios, whole-cell biocatalysis is advantageous over in vitro systems (Duetz et al., 2001; Schmid et al., 2001). Multi-step transformations involving several enzymes in a biosynthetic pathway, and metabolite overproduction coupled to breakdown of a growth substrate both demand the use of whole-cell systems. Use of whole cells also offers the opportunity to regenerate via sugar metabolism the reduced cofactors that are used to drive heterologous redox reactions of interest. However, there is significant room for improvement in the "efficiency" with which glucose or other sugars are utilized as "cosubstrates" for providing the reducing power required to drive these

Correspondence to: P.C. Cirino

Contract grant sponsor: NSF
Contract grant number: BES0519516

reactions. That is, the quantity of reducing equivalents derived from cosubstrate oxidation that are actually used by the heterologous reaction is far from the theoretical maximum, as described below and elsewhere (Cirino et al., 2006).

Several strategies have been employed to improve the availability of NADPH in whole cells. Moreira dos Santos et al. (2004) reported the use of $NADP^+$-dependent malic enzymes to increase cytosolic or mitochondrial levels of NADPH within *Saccharomyces cerevisiae*. Weckbecker and Hummel (2004) overexpressed the membrane-bound transhydrogenase PntAB in *Escherichia coli* to improve the NADPH-dependent conversion of acetophenone to (*R*)-phenylethanol. Sanchez et al. (2006) overexpressed the soluble transhydrogenase SthA in *E. coli* to improve the NADPH-dependent production of poly(3-hydroxybutyrate). Verho et al. (2003) reported an increase in ethanol yield from pentose sugars in an *S. cerevisiae* strain by overexpressing an $NADP^+$-dependent glyceraldehyde 3-phosphate dehydrogenase (*GPD1*) from *Kluveromyces lactis*.

We previously reported xylitol-producing *E. coli* strain PC09 (*crp**, Δ*xylB*) expressing NADPH-dependent xylose reductase from *Candida boidinii* (CbXR). The use of a cAMP-independent CRP mutant (*crp**) enables co-uptake of glucose and xylose, while the *xylB* (xylulokinase) deletion prevents xylose metabolism. We were interested in increasing the availability of NADPH for xylose reduction, which we defined as the moles of xylitol produced per mole of glucose consumed (Y_{RPG}), and showed that this value was increased from 1.8 in batch culture to >3.7 in resting cells (Cirino et al., 2006). The current study aims to understand which metabolic pathways are primarily responsible for supplying NADPH to the xylose reductase, as a step toward increasing the availability of NADPH for driving heterologous reactions in whole-cell biocatalysts.

We first combined stoichiometric metabolic network modeling with knowledge of xylose transport and central metabolism to study how key enzymes influence the xylitol yield. Mutant strains were next created to investigate the contribution of particular pathways or reactions toward xylitol yield. Genes that were studied are shown in Figure 1 and include *pgi* (encoding phosphoglucose isomerase), *zwf* (glucose 6-phosphate-1-dehydrogenase), *ndh* (NADH dehydrogenase II), *sucC* (succinyl-CoA synthetase), *edd-eda* (phosphogluconate dehydrogenase and 2-keto-3-deoxy-6-phosphogluconate aldolase, respectively), and the transhydrogenase genes *sthA* and *pntA*. Also, plasmid-based overexpression of the transhydrogenases was examined as a potential means of increasing NADPH supply. Resting cell assays were used to compare the strains in this study because xylitol production is growth-uncoupled and this assay permitted accurate comparisons between non-growing biocatalysts that display widely different growth characteristics. We found that the strain lacking *pgi* has an improved yield compared to strain PC09. Deleting the genes *zwf*, *ndh*, or *sucC* drastically reduces the yield, whereas deletion of the transhydrogenases does not affect yield and functional overexpression of either transhydrogenase does not improve the yield.

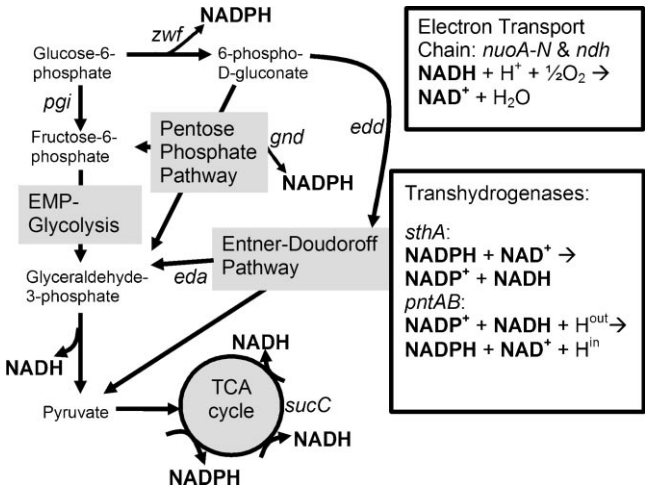

Figure 1. *E. coli* central carbon metabolism summarizing key reactions and pathways involved in NAD(P)H metabolism. Genes shown code for the following enzymes: *pgi* = phosphoglucose isomerase; *zwf* = glucose 6-phosphate-1-dehydrogenase; *gnd* = 6-phosphogluconate dehydrogenase; *edd* = phosphogluconate dehydratase; *eda* = 2-keto-3-deoxy-6-phosphogluconate aldolase; *nuoA-N* = NADH dehydrogenase I; *ndh* = NADH dehydrogenase II; *sucC* = succinyl-CoA synthetase; *sthA* = soluble pyridine nucleotide transhydrogenase; *pntAB* = pyridine nucleotide transhydrogenase. Pathway abbreviations include the following: EMP = Embden-Meyerhof-Parnas, TCA = tricarboxylic acid.

Materials and Methods

General

Strains and plasmids used in this study are listed in Table I. *E. coli* W3110 (ATCC 27325) and derivative strains were maintained on plates containing either Luria-Bertani (LB) medium, or minimal medium containing mineral salts (per liter: 3.4 g KH_2PO_4; 5.2 g K_2HPO_4; 3.3 g $(NH_4)_2HPO_4$, 0.25 g $MgSO_4 \cdot 7\ H_2O$, 15 mg $CaCl_2 \cdot 2\ H_2O$, 0.5 mg thiamine, and 1 mL of trace metal stock), glucose (2%), and 1.5% agar. The trace metal stock was prepared as described (Causey et al., 2003). 4-Morpholinopropanesulfonic acid (MOPS) was added to liquid media for pH control (50 mM, pH 7.4). Antibiotics were included as required (kanamycin sulfate, 50 $\mu g\,mL^{-1}$; ampicillin, 100 $\mu g\,mL^{-1}$; apramycin sulfate, 50 $\mu g\,mL^{-1}$; chloramphenicol, 50 $\mu g\,mL^{-1}$) and isopropyl-β-D-thiogalactopyranoside (IPTG) (100 μM, unless otherwise noted) was used to induce gene expression under *tac* promoter (p_{tac}) control. Xylitol, xylose, xylulose, glucose, and organic acid concentrations were determined using a Shimadzu LC-10AD HPLC equipped with a UV monitor (210 nm) and refractive index detector (RID). Products were separated using a Bio-Rad HPX-87H column operated at

Table I. Strains and plasmids used in this study*

	Relevant characteristic	References
Strain		
W3110	Wild-type	ATCC 27325
PC09	*crp**, Δ*xylB*::FRT (Tet^R)	Cirino et al. (2006)
PAP01	W3110, Δ*pntA*:: FRT-*kan*-FRT (Kan^R)	This study
CF13	W3110, Δ*sucC*:: FRT-*kan*-FRT (Kan^R)	This study
JC16	PC09, CbXR integrated at HK022 (Tet^R, Apr^R)	This study
JC17	PC09, CbXR integrated at HK022 (Tet^R)	This study
JC38	W3110, Δ*sthA*:: FRT-*kan*-FRT (Kan^R)	This study
JC53	W3110, Δ*pgi*:: FRT-*kan*-FRT (Kan^R)	This study
JC54	W3110, Δ*zwf*:: FRT-*kan*-FRT (Kan^R)	This study
JC62	BW25142 Δ*zwf-eda*:: FRT-*aac*-FRT (Apr^R)	This study
JC63	BW25142 Δ*edd-eda*:: FRT-*aac*-FRT (Apr^R)	This study
JC68	W3110, Δ*zwf-eda*:: FRT-*aac*-FRT (Apr^R)	This study
JC69	W3110, Δ*edd-eda*:: FRT-*aac*-FRT (Apr^R)	This study
Plasmid		
pLOI3809	*kan*, pBR322-origin vector for heterologous gene expression under control of *tac* promoter	Cirino et al. (2006)
pLOI3815	pLOI3809 carrying xylose reductase from *Candida boidinii* (CbXR)	Cirino et al. (2006)
pPCC05	pLOI3809 carrying xylose reductase from *Candida tenuis* (CtXR)	Cirino et al. (2006)
pPCC09	pLOI3809 carrying *sthA* gene from W3110	This study
pPCC102	pLOI3809 carrying *pntAB* gene from W3110	This study
pPCC106	pLOI3815 with *pntAB* from pPCC102	This study
pPCC107	pLOI3815 with *xylE* from pPCC203	Khankal et al. (2008)
pPCC203	pLOI3809 carrying *xylE* gene from W3110	Khankal et al. (2008)
pPCC205	pLOI3809 carrying *xylFGH* gene from W3110	Khankal et al. (2008)
pPCC207	pLOI3815 with *xylFGH* from pPCC205	Khankal et al. (2008)
pPCC500	pLOI3815 with *sthA* gene from pPCC09	This study

Other gene deletion strains described are derived from strain PC09.
*Tet, tetracycline; Kan, kanamycin; Apr, apramycin.

45°C with a mobile phase of 4 mM H_2SO_4 at a flow rate of 0.5 mL min^{-1}. Cell culture optical density was measured spectrophotometrically at 600 nm (OD_{600}). Cell dry weight (cdw) was calculated to be 0.33 g L^{-1} for OD_{600} at 1.0.

Standard methods were used for plasmid construction, phage P1 transduction, electroporation, and polymerase chain reaction (PCR) (Miller, 1992; Sambrook and Russell, 2001). Strain JC17 was created by integrating a fragment of plasmid pLOI3815 (containing the *lacI* gene, *tac* promoter, *CbXR* gene, and terminator region) into the genome of PC09 using the CRIM method described by Haldimann and Wanner (2001). The FRT-flanked *bla* gene in plasmid pAH68 (Haldimann and Wanner, 2001) was first replaced with the *aac* gene as follows. The *aac* gene was isolated by digesting lab plasmid pLOI3821 with *Sma*I, and was ligated into plasmid pAH68 which had been digested with *Msl*I and phosphotase treated. The resulting plasmid is pPCC20. Plasmid pLOI3815 was digested with *Fsp*I and a 4.4 kb fragment, containing the relevant genes, was isolated and ligated into pPCC20, which had been digested with *Sma*I and treated with CIP (calf intestinal alkaline phosphatase). The resulting plasmid is pPCC100. pPCC100 was subsequently integrated into the chromosome of PC09 at the HK022 site resulting in JC16. Apramycin resistant colonies arising from the successful integration of the pPCC100 region were selected and verified by PCR. Removal of the FRT-flanked apramycin resistance cassette was performed as described (Causey et al., 2003), resulting in strain JC17.

Gene Deletions

E. coli K-12 strains with single gene deletions carrying an FRT-flanked kanamycin resistance cassette in place of the selected gene (*pgi*, *zwf*, *pntA*, *sthA*, *sucC*, *ndh*) were obtained from the Keio collection (Baba et al., 2006). P1 phage transductions were performed to propagate the gene deletions. Combined deletions in the *zwf-eda*, and *edd-eda* genes were constructed using the one-step inactivation method described by Datsenko and Wanner (2000). Briefly, apramycin resistance gene (*aac*) flanked by FRT flipase recognition sequences (in lab plasmid pLOI3421) was PCR-amplified using the primer pairs: "zwf for" (ACG GGT GGA TAA GCG TTT ACA GTT TTC GCA AGC TCG TAA-GGC GAT TAA GTT GGG TAA CG) and "eda rev" (GAC TTT TAC AGC TTA GCG CCT TCT ACA GCT TCA CGC GCC-TTC CGG TCT CCC TAT AGT GA) or "edd for" (CGT GCG GAT TCA CCC ACG AGG CTT TTT TTA TTA CAC TGA-GGC GAT TAA GTT GGG TAA CG) and "eda rev." The underlined portions represent the region homologous to plasmid pLOI3421. The non-underlined portions are homologous to the chromosomal location corresponding to ~120 bp upstream of the *zwf* start codon (zwf for), ~150 bp

upstream of the *edd* start codon (eda for), and overlapping the stop codon of *eda* (eda rev). The PCR products were electroporated into strain BW25142 expressing the λ-red recombinase from plasmid pKD46 (Causey et al., 2003). Chromosomal deletions were verified by colony PCR. All FRT-flanked antibiotic resistance markers were removed using flipase recombinase (Causey et al., 2003).

Transhydrogenase Expression Plasmids

The *pntA-pntB* gene segment and *sthA* gene were amplified from *E. coli* W3110 genomic DNA (performed in a Bio-Rad iCycler thermocycler using iProof high fidelity polymerase (Bio-Rad)). Primers for *pntAB* amplification were: "pntA for *Hin*dIII," 5′-CGT AAG CTT CCG ATG GAA GGG AAT ATC ATG-3′ (*Hin*dIII underlined); "pntB rev *Kpn*I" 5′-ATC GGT ACC CAG GGT TAC AGA GCT TTC AG-3′ (*Kpn*I underlined). The resulting PCR product was digested with *Hin*dIII and *Kpn*I and ligated into lab expression vector pLOI3809 which had been digested with the same two restriction enzymes, creating plasmid pPCC102. Primers for the *sthA* amplification were: "sthafor1," 5′-CTA GCT CGA GCC GGC GGC GAA GGC GCT GC-3′ (*Xho*I underlined); "stharev1," 5′-CTA CGG TAC CCA AGA ATG GAT GGC CAT TTC G-3′ (*Kpn*I underlined). The resulting PCR product was digested with *Xho*I and *Kpn*I then ligated to the 6.4 kb fragment isolated from lab plasmid pPCC02 which had been digested with the same two enzymes, creating plasmid pPCC09.

Plasmids pPCC106 and pPCC500 were created as follows: the *pntAB* gene segment from pPCC102 was prepared by digesting the plasmid with the *Hin*dIII, Klenow treating, digesting with *Bgl*II, and then isolating the 2.9 kb fragment via gel purification. The PntAB fragment was ligated into pLOI3815, which had been digested with *Sma*I and *Bgl*II, resulting in plasmid pPCC106. The *sthA* gene was isolated from pPCC09 after digesting the plasmid with *Kpn*I and *Xho*I. The purified 1.4 kb fragment was ligated into pLOI3815 vector, which had been previously digested with the same enzymes, resulting in pPCC500.

Shake-Flask Cultures

All cultures were performed in at least duplicates. Shake-flask cultures for xylitol production were performed as previously described (Cirino et al., 2006). Briefly, seed cultures were prepared by inoculating with a few colonies from a fresh plate (LB plates for LB cultures, minimal medium plates containing 2% glucose for minimal medium cultures) into three mL of medium. Seeds were grown to an OD_{600} of 2.0–4.0, and shake-flask cultures were inoculated directly from the seed cultures by dilution to a final OD_{600} of 0.1. Cells were grown in 50 mL of medium in a 250 mL baffled Erlenmeyer flask grown at 30°C and 250 rpm.

Resting Cell Cultures

Resting cells were prepared using a protocol similar to that described by Walton and Stewart (2004) and Cirino et al. (2006). Briefly, 25 mL seed cultures were grown in either minimal medium or LB medium at 37°C to a final OD_{600} of 1.0–4.0 and used to inoculate 200 mL cultures to an initial OD_{600} of 0.05 in either minimal medium or LB medium supplemented with 50 mM xylose and 100 mM glucose in a 1 L Erlenmeyer flask. This culture was induced with 100 μM IPTG at inoculation, and shaken at 250 rpm and 30°C. When the cells reached an OD_{600} between 2.0 and 4.0 (exponential growth), chloramphenicol was added to the culture to inhibit further protein synthesis. Cells harvested in this growth stage were previously determined to behave reproducibly in resting culture and give stable yields for at least 48 h (Cirino et al., 2006). The culture was then harvested by centrifugation, washed in minimal medium lacking a carbon and nitrogen source and resuspended to a final OD_{600} of 2.0 in minimal medium lacking nitrogen but containing an appropriate amount of sugar (50 mM glucose and/or 300 mM xylose). Aerated resting cell experiments used 30 mL of resuspended cells in 250 mL baffled flasks shaking at 250 rpm and 30°C. Oxygen-limited resting cell experiments used 30 mL of resuspended cells in 250 mL baffled flasks sitting in an incubator at a controlled temperature of 30°C. All resting cell tests were performed in at least duplicate and reported values represent the averages after 24 h of resting cell biotransformation. Confidence intervals represent the standard deviation. Molar yields of xylitol per glucose consumed (Y_{RPG}), were calculated as described previously (Cirino et al., 2006); briefly, xylitol production levels were corrected for the xylitol produced in the absence of glucose, before normalizing with respect to glucose consumption levels.

Transhydrogenase Activity Assay

Cells were grown in 50 mL of LB medium supplemented with 50 mM glucose, in a 250 mL baffled Erlenmeyer flask. The cultures were harvested at OD_{600} between 3.0 and 4.0 by pelleting the cells and washing twice with 0.9% (w/v) NaCl and 10 mM $MgSO_4$. Cell pellets were stored at −20°C until use. The cell pellet was resuspended to an OD_{600} of 12.5 in lysis buffer (100 mM Tris–HCl pH 7.5, 5 mM $MgCl_2$, 3.33 $\mu g\,mL^{-1}$ DNase I, Protease Arrest (G Biosciences, St. Louis, MO used at ½ manufacturer's recommended concentration), 0.2 mM dithiothrietol). The cell pellet was lysed by two passes through a French Pressure cell press and subsequently centrifuged at 4°C, 13,000 rpm, for 5 min to remove cellular debris. The resulting supernatant contained both the soluble and membrane-bound transhydrogenases. To isolate the membrane, the lysates were further centrifuged at 50,000*g* for 60 min at 4°C (via ultracentrifugation) and the resulting pellets were resuspended in a volume equal to the initial sample of 50 mM sodium phosphate buffer pH 7.0.

Transhydrogenase activity was measured according to the following procedure adapted from Sauer et al. (2004) in a 96-well microtiter plate using a Spectra Max Plus^{384} plate reader. Reactions contained different amounts of cell lysate in 200 μL total volume with 50 mM Tris–HCl pH 7.5, 2.0 mM $MgCl_2$, 2.0 mM β-NADPH, 2.0 mM 3-acetyl pyridine adenine dinucleotide ($APAD^+$). $APAD^+$ is an analogue of NAD^+; the concentration of its reduced form (APADH) was readily determined by absorbance at $\lambda =$ 400 nm (extinction coefficient ~2.9 $(mM\,cm)^{-1}$ (Ciotti and Kaplan, 1956)) with minimal absorbance interference from β-NADPH. Absorbance was monitored for 1 min with readings taken every 2 s. One unit (U) is defined as the activity that produces 1 μmol of APADH in 1 min.

CbXR Activity Assay

Seed cultures (10 mL in LB medium) were grown to an OD_{600} of ~2.0, and were used to inoculate cultures by dilution to a final OD_{600} of 0.1 in 125 mL of LB medium supplemented with 50 mM glucose, and 100 or 300 μM IPTG in a 1-L Erlenmeyer flask. When the cultures reached an OD_{600} of 2.0–3.0, the cells were harvested by pelleting and washed twice with 25 mL of 50 mM potassium phosphate buffer pH 7.5. The cell pellets were stored at −20°C until use. The cell pellets were resuspended to a final OD_{600} of 50 in lysis buffer (50 mM potassium phosphate buffer pH 7.5, 4.0 mM $MgCl_2$, 3.3 $\mu g\,mL^{-1}$ DNase I, Protease Arrest (G Biosciences, St. Louis, MO used at ½ manufacturer's recommended concentration)). The cell pellet was lysed by two passes through a French Pressure cell press and subsequently centrifuged at 4°C, 13,000 rpm, for 60 min to remove cellular debris. The resulting supernatant contained the xylose reductase.

Xylose reductase activity was measured in a 96-well microtiter plate. Reactions contained 300 mM xylose, 300 μM β-NADPH, 50 mM potassium phosphate buffer pH 7.5, and cell lysate supernatant in 200 μL total volume. Reduction in the β-NADPH concentration was readily determined by absorbance at $\lambda = 340$ nm (extinction coefficient ~6.2 $(mM\,cm)^{-1}$). One unit (U) is defined as the activity that consumes one μmol of NADPH in 1 min (background activity in the absence of xylose is subtracted).

Simulations

A genome-scale constraints-based metabolic model, as described by Reed et al. (2003), was adapted to examine xylitol production. Linear optimization was used to find a solution that maximized the production of xylitol. Simulation of gene deletion mutant strains was accomplished by setting the flux through the corresponding gene product(s) to zero, as described by Covert and Palsson (2002). Sauer and Canonaco demonstrated that the energy-independent soluble transhydrogenase (SthA) converts NADPH to NADH (Canonaco et al., 2001; Sauer et al., 2004); therefore the SthA-catalyzed reaction was constrained to be irreversible in the direction of NADH production. The energy-dependent membrane-bound transhydrogenase (PntAB) was assumed to be irreversible in the direction of NADPH formation, as suggested by Sauer et al. (2004). Though Pgi is known to be reversible (e.g., during gluconeogenesis) (Hua et al., 2003), metabolic flux analysis suggests that the net flux through Pgi during glucose metabolism is in the direction of glycolysis (Hua et al., 2003; Sauer et al., 2004) and Zhao and Shimizu (2003) have shown limited flux through Pgi in the reverse direction (fructose-6-phosphate to glucose-6-phosphate) when grown on acetate. This led to an added model constraint that restricts flux through Pgi in the reverse direction to be, at most, equal to the flux necessary for biomass production. An ATP maintenance reaction with a flux of 7.6 mmol ATP $(g\,cdw\,h)^{-1}$ was also included in all simulations (Reed et al., 2003; Varma and Palsson, 1994). To allow for xylitol production, an irreversible NADPH-dependent xylose reduction reaction was added to the model, as well a xylitol diffusion pathway that allowed for xylitol secretion. An energy-independent diffusion pathway was chosen because no known xylitol-specific transporters exist in *E. coli*, though xylitol has been shown to be transported by glycerol facilitator (GlpF) (Heller et al., 1980). The added reactions are as follows:

$$\text{Xylitol production} - \text{Xylose (int)} + H^+\text{(int)} + \text{NADPH} \rightarrow \text{Xylitol (int)} + NADP^+$$

$$\text{Xylitol secretion} - \text{Xylitol (int)} \rightarrow \text{Xylitol (ext)}$$

Results

Effect of Growth Medium on Resting Cell Yield

In our previous study minimal medium was used to grow cultures prior to preparation of resting cells (Cirino et al., 2006). With that protocol, the Y_{RPG} for strain PC09 harboring plasmid pLOI3815 (medium-copy, used for expression of *C. boidinii* xylose reductase (CbXR)) ranged between 3.8 and 4.0 over a 48 h period under highly aerated conditions. Secretion of by-products such as acetate or lactate was minimal under optimal xylitol production conditions. Reduced aeration reduced the xylitol yield and resulted in incomplete glucose oxidation and secretion of fermentation products. Several of the gene deletion strains used in the current study exhibited poor growth on minimal glucose medium, as also reported by others (Hua et al., 2003; Sauer et al., 2004; Zhao et al., 2004). To avoid drastic growth differences between strains (e.g., culture time prior to harvesting) and selective pressures that may lead to compensatory mutations, we chose to compare resting cell performance of these strains by culturing them in rich (Luria-Bertani) medium (supplemented with 50 mM xylose and 100 mM glucose), rather than a minimal medium; the minimal resting cell medium remained unchanged and is

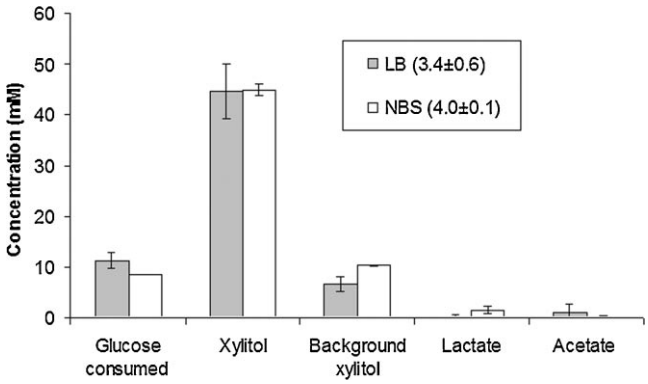

Figure 2. Comparison between resting cell results using strain PC09 harboring plasmid pLOI3815 (expressing CbXR) that was first cultured in rich medium (LB) versus minimal medium (NBS). The corrected Y_{RPG} is shown in parenthesis.

free of a nitrogen source. In this study, experimental yield values were determined after 24 h of biotransformation, although yields generally remained constant for at least 48 h.

As shown in Figure 2, the yield of reference strain PC09 was reduced as a result of growth in LB (3.4 vs. 4.0 at 24 hours), while secretion of by-products remained minimal. Thus, the "reference" yield in this study is 3.4. The increased Y_{RPG} observed from cells grown in minimal medium (compared to LB-glucose) may be a result of higher flux through catabolic pathways producing NADPH for biosynthesis during growth, lower expression of genes involved in aerobic respiration (Tao et al., 1999), and/or higher total TCA cycle activity compared to cells grown in complex medium supplemented with glucose (Gray et al., 1966). Resting cells prepared without an energy source (glucose) produce low, "background" levels of xylitol, and when calculating Y_{RPG} this background level of production was subtracted from the amount produced in the presence of glucose. As shown in Figure 2, the background production of xylitol is 56% higher for cells grown in minimal medium compared to cells grown in LB (10.5 mM vs. 6.7 mM). This may be a result of increased production of carbohydrate reserves during growth in minimal glucose medium.

Role of Xylose Transport and CbXR Expression

To determine whether xylose transport and in vivo availability to the reductase could be limiting the yield, we tested the effect of overexpressing the xylose-proton symporter XylE in PC09. The XylE gene (*xylE*) was cloned downstream of the CbXR gene in pLOI3815 such that both genes were controlled by the *tac* promoter, yielding bicistronic plasmid pPCC107 (Khankal et al., 2008). This plasmid enabled xylose uptake and high levels of xylitol production in the presence of glucose in strain PC07 (W3110, Δ*xylB*, wild-type *crp*), verifying functional expression of XylE (xylitol production was low in PC07 carrying pLOI3815) (Khankal et al., 2008). In contrast, resting cell Y_{RPG} and xylitol production in batch cultures of PC09 (PC07, *crp**) harboring pPCC107 were not improved relative to PC09 carrying pLOI3815 (not shown), suggesting xylose transport does not impose a significant limitation to xylitol production in this strain (CRP* in PC09 enables expression of xylose transporters in the presence of glucose, and added overexpression of XylE is of no benefit). The same observation was made when the ATP-binding cassette-type xylose transporter XylFGH (rather than XylE) was co-expressed with CbXR from plasmid pPCC207 (also verified to enable xylitol production in PC07 (Khankal et al., 2008)).

We next tested whether xylitol yield is limited by the expression level of CbXR. Strain JC17 is similar to PC09 but contains a single, chromosomally-integrated copy of the CbXR gene (under p_{tac} control). We compared resting cell yields and xylose reductase activities (measured from cell lysates) for strains JC17 and PC09 harboring pLOI3815, after having been induced with IPTG during growth (300 μM for JC17, 100 μM for PC09). Although PC09 carrying pLOI3815 had almost twofold higher specific xylose reductase activity compared to JC17 (~400 mU (mg total protein)$^{-1}$ compared to ~210 mU (mg total protein)$^{-1}$), the yields were very similar (yield was actually slightly lower in PC09, which may reflect metabolic changes due to plasmid maintenance). Increasing the IPTG concentration to 300 μM during growth of PC09 + pLOI3815 resulted in a further ~70% increase in CbXR activity in the lysate without an increase in resting cell yield.

These initial studies suggested that availability of xylose and enzyme do not significantly limit the molar xylitol yield in strain PC09. Nonetheless, the yield obtained from resting cells (~3.4) is significantly lower than the theoretical maximum yield (which depends on the metabolic network, as discussed below). NADPH availability therefore seems likely to be limiting the reduction of xylose to xylitol. Another strong indication that NADPH availability limits the xylitol yield is the fact that the yield obtained from minimal medium batch cultures (~1.8) is significantly lower than that obtained from resting cell cultures, where NADPH is no longer consumed in anabolic reactions. We next turned to stoichiometric modeling of *E. coli* metabolism to better understand energy- and pathway-related factors that contribute to NADPH availability and yield in this system.

Simulation Studies

Beginning from an *E. coli* genome-scale stoichiometric metabolic network (Covert and Palsson, 2002; Reed et al., 2003; Varma and Palsson, 1994), strain PC09 was simulated by eliminating the xylulokinase reaction (XylB) and allowing unlimited xylose uptake. Reactions for NADPH-dependent xylose reduction to xylitol and energy-free xylitol transport were also added to the stoichiometric network. Additional modeling details are described in Materials and

Methods Section. With glucose uptake fixed at 10 mmol glucose $(g\,cdw\,h)^{-1}$, xylitol production was set as the optimization objective function (maximization). The maximum theoretical yield corresponds to the resulting xylitol flux normalized with respect to glucose consumption. Table II summarizes the maximum xylitol yield results from simulations with PC09 and select mutant strains, and indicates the sources of NADPH leading to these yields. The maximum theoretical yield in PC09 is 9.2. As expected, the less energy-demanding xylose-proton symporter (XylE) was chosen over the ATP-dependent xylose transport system (XylFGH). Fixing all xylose uptake through XylFGH lowered the maximum theoretical yield to 6.9. Major contributors to NADPH supply are the pentose phosphate (PP) pathway (Zwf and Gnd enzymes), the tricarboxylic acid (TCA) cycle (Icd), and the proton-translocating transhydrogenase PntAB, which is consistent with the findings of Sauer et al. (2004). Flux through Pgi and the soluble transhydrogenase (SthA) were zero when xylitol production was maximized in the model.

The primary physiological role of PntAB is believed to be the transfer of reducing equivalents from NADH to NADPH (Sauer et al., 2004), and PntAB is therefore a potential source of NADPH for xylose reduction. Upon deletion, the model predicted that the maximum theoretical yield decreased to 3.6, which is equivalent to the net supply of NADPH derived from the PP pathway and TCA cycle. In contrast, SthA is believed to primarily catalyze the conversion of NADPH to NADH (Canonaco et al., 2001; Sauer et al., 2004). A deletion in the *sthA* gene could therefore potentially increase xylitol yield by eliminating a drain of NADPH. Note, however, that deleting SthA from the model did not impact the theoretical maximum yield. Deleting either *pgi* or *zwf* perturbs NADPH metabolism since these gene products determine the fate of glucose-6-phosphate (Hua et al., 2003; Sauer et al., 2004). A *pgi* mutation forces glucose-6-phosphate oxidation through the PP and Entner-Doudoroff (ED) pathways and has been implicated in generating excess NADPH, as suggested by an observed slower growth rate (Hua et al., 2003; Sauer et al., 2004). A *zwf* mutation forces glucose metabolism through the Embden-Meyerhof-Parnas (EMP) pathway. This mutant strain has a lower maximum theoretical yield due to the added energy requirements for PntAB-dependent NADPH production from the reducing equivalents generated (NADH) through EMP. A mutant strain with a nonfunctional TCA cycle was modeled by removing the SucC reaction. As with the Zwf mutant, NADPH production is compensated by an increased flux through the PntAB reaction, resulting in a decreased maximum theoretical yield.

Table II. Predicted maximum theoretical yield and NADPH source(s) from simulated strains used in this study.*

Strain	Xylitol (yield)	Source of NADPH		
		PPP	TCA	PntAB
PC09	9.2	2.0	1.7	5.6
Δ*pnt*	3.6	2.0	1.7	0.0
Δ*zwf*	8.8	0.0	1.7	7.2
Δ*pgi*	9.2	2.0	1.7	5.6
Δ*sthA*	9.2	2.0	1.7	5.6
Δ*ndh*, Δ*nuoA-N*	9.0	2.0	1.7	5.4
Δ*xylE*	6.9	2.0	1.7	3.3
ΔTCA(*sucC*)	8.0	2.0	0.0	6.0
Δ*pgi*, Δ*sthA*	9.2	2.0	1.7	5.6
Δ*pntAB*, Δ*zwf*	1.8	0.0	1.8	0.0
Δ*pntAB*, Δ*pgi*	3.6	2.0	1.7	0.0
Δ*pntAB*, Δ*sthA*	3.6	2.0	1.7	0.0
Δ*pntAB*, ΔTCA(*sucC*)	2.8	2.0	0.8	0.0

Model constraints and parameters are descried in the Materials and Methods Section.

*NADPH source may not match the xylitol yield due to rounding error and drain for minimal biomass formation constraint (0.0092 g biomass $(g\,cdw\,h)^{-1}$).

Resting Cell Assays

To better understand the contributions of the central carbon metabolism reactions discussed above toward NADPH supply and xylitol yield in resting cells, variants of strain PC09 were next constructed and tested experimentally. Table III lists the Y_{RPG} values and amounts of glucose consumed and metabolites secreted after 24 h of resting cell biotransformation by these strains. Y_{RPG} from the control strain PC09 (~3.4) is significantly lower than the predicted value of either 9.2 (assuming xylose transport through XylE) or 6.9 (assuming xylose transport through XylFGH). This is due, in small part, to the incomplete oxidation of glucose (indicated by the secretion of pyruvate, lactate, and acetate by-products). Table IV lists "adjusted" maximum theoretical yield values in which glucose consumption and metabolite secretion profiles were incorporated as constraints to the model. These adjusted theoretical values are listed both for the case of XylE- and XylFGH-mediated xylose transport. Note that the decrease in maximum yield for most strains tested is not significant, since the acid by-products represent a small fraction of total glucose consumed. Thus, the experimentally achieved Y_{RPG}'s are still significantly lower than the maximum theoretical yields.

EMP/PP/ED Mutants

Of the gene deletion strains tested, JC72 (Δ*pgi*) had the highest Y_{RPG} (~4.0). This suggests that some glucose-6-phosphate is directed through Pgi (EMP) in PC09 resting cells, and diverting flux away from Pgi and through Zwf (ED and/or PP) results in increased NADPH availability for xylitol production. A slower glucose uptake rate and slower growth rate due to a *pgi* mutation have been reported (Blank et al., 2008; Hua et al., 2003; Sauer et al., 2004), and are likely due to a decreased rate of oxidized cofactor regeneration. The slight reduction in glucose uptake rate for JC72 compared to PC09 is in agreement with these observations.

Table III. Experimental results from resting cell biotransformations for the various strains described.

Strain	Relevant genotype	Y_{RPG}	Glucose (mM)	Xylitol (mM)	Acetate (mM)	Pyruvate (mM)	Lactate (mM)	Bkgd Xylitol (mM)
PC09	Reference	3.4 ± 0.6	11.3 ± 1.5	44.6 ± 5.4	1.3 ± 1.4	0.0 ± 0.0	0.2 ± 0.4	6.7
JC72	Δ*pgi*	4.0 ± 0.4	8.3 ± 0.8	44.0 ± 4.6	0.3 ± 0.3	0.0 ± 0.0	0.5 ± 0.9	10.6
JC73	Δ*pntA*	3.6 ± 0.4	9.1 ± 1.5	40.0 ± 5.8	1.4 ± 1.5	0.1 ± 0.2	0.3 ± 0.5	6.4 ± 1.2
JC74	Δ*sthA*	3.6 ± 0.4	10.9	46.0 ± 4.5	3.1 ± 0.8	0.0 ± 0.0	0.0 ± 0.0	9.1 ± 1.4
JC75	Δ*zwf*	2.0 ± 0.3	11.4 ± 1.7	30.7	6.9 ± 1.3	0.1 ± 0.2	0.4 ± 0.5	8.1 ± 1.3
JC79	Δ*ndh*	0.6 ± 0.2	21.2	18.8 ± 6.0	4.0 ± 0.5	20.4 ± 4.5	15.2 ± 7.7	5.7 ± 1.9
MR02	Δ*pntA*, Δ*sthA*	3.5 ± 0.6	12.3 ± 2.3	48.1	2.0 ± 2.2	0.1 ± 0.0	0.1 ± 0.1	5.4 ± 1.0
JC87	Δ*sucC*	2.3 ± 0.3	12.5 ± 1.2	41.2	6.9 ± 2.7	1.2 ± 1.3	0	9.9 ± 5.4
JC88	Δ*pgi*, Δ*sthA*	4.2 ± 0.7	7.1	41.7 ± 4.5	1.7 ± 0.3	0.1 ± 0.0	0	11.4
pPCC107[a]	*xylE*$^+$	2.0 ± 0.7	7.8	18.5 ± 4.0	6.7	0.4 ± 0.4	0.5 ± 0.2	3.8 ± 1.3
pPCC207[a]	*xylFGH*$^+$	1.9 ± 1.1	12.7 ± 2.0	37.6 ± 8.9	3.5 ± 2.1	0.0 ± 0.0	0.3 ± 0.5	6.3 ± 1.7
pPCC106[a]	*pntAB*$^+$	1.2 ± 0.5	12.8	17.7 ± 6.1	11.6 ± 2.9	0.2 ± 0.1	0.1 ± 0.1	3.8 ± 1.2
pPCC500[a]	*sthA*$^+$	2.8 ± 0.3	10.4	32.6 ± 3.3	4.6 ± 1.1	0.1 ± 0.1	0.3 ± 0.5	4.8 ± 0.7

Y_{RPG} is corrected for the background production of xylitol in the absence of glucose (given as "Bkgd Xylitol"). Standard deviations were less than 10% of the average unless indicated.

[a]Plasmid used to co-express the indicated gene(s) with CbXR in strain PC09.

As with PC09, the amount of by-products secreted is a small fraction of the glucose consumed.

Zwf and Gnd play important roles in contributing NADPH for xylitol production in PC09. As shown in Table III, Y_{RPG} for JC75 (Δ*zwf*) is reduced to 2.0, which is approximately 40% decreased compared to PC09 and 50% lower than JC72. The glucose consumption rate for JC75 was similar to that for PC09, but JC75 secreted more acetate and less xylitol. Because a higher fraction of glucose carbon was secreted as acid by-products, the theoretical maximum yield decreased more significantly upon adjustment for by-products (Table IV), although the adjusted yield (5.3 for xylose transport via XylFGH) was still much higher than the experimentally determined Y_{RPG}. Whereas deletion of Zwf in the model causes only a mild reduction in the theoretical maximum xylitol yield (due to elevated flux through PntAB), the deletion has a much more significant impact on the experimental Y_{RPG}. Though not generally used by *E. coli* growing on glucose (Flores et al., 2002; Hua et al., 2003; Sauer et al., 2004), the ED pathway was deleted in conjunction with the *pgi* and *zwf* gene deletions to ensure complete flux through either the PP or EMP pathway, respectively. Mutant strains JC94 (Δ*pgi*, Δ*edd-eda*) and JC76 (Δ*zwf*, Δ*edd-eda*) had Y_{RPG} values comparable to JC72 and JC75, respectively (data not shown).

TCA Cycle and Respiration Mutants

The nearly complete oxidation of glucose in resting cells suggests a functional TCA cycle. Inactivation of a complete TCA cycle by deleting *sucC* (strain JC87) significantly lowers the experimental Y_{RPG} (2.3) compared to PC09. As shown in Table III, the glucose consumption rate in JC87 was similar to that in PC09, but JC87 produced more acetate and pyruvate. These results are expected since acetyl-CoA can no longer be oxidized through the TCA cycle (Bock and Sawers, 1996) (aerated conditions prevent diversion of carbon to fermentation products) and indicate that a functional TCA cycle contributes to NADPH availability for xylitol production in PC09.

Strain JC79 containing a deletion in *ndh* (NADH dehydrogenase II) was created to determine whether reducing NADH oxidation via respiration would feed back into increased NADPH availability. As shown in Table III, the resulting Y_{RPG} was only 0.6, due largely to incomplete oxidation of glucose. The observed high levels of pyruvate

Table IV. Predicted maximum theoretical yields adjusted for experimentally determined glucose uptake and metabolite secretion profiles (reported in Table III).

Strain	XylE simulated	XylE adjusted simulated	XylFGH simulated	XylFGH adjusted simulated	Y_{RPG} experimental
PC09	9.2	9.2	6.9	6.8	3.4 ± 0.6
JC72 (Δ*pgi*)	9.2	8.8	6.9	6.3	4.0 ± 0.4
JC73 (Δ*pntA*)	3.6	3.4	3.6	3.4	3.6 ± 0.4
JC74 (Δ*sthA*)	9.2	8.4	6.9	6.1	3.6 ± 0.4
JC75 (Δ*zwf*)	8.8	7.2	6.7	5.3	2.0 ± 0.3
JC79 (Δ*ndh*)	9.0	1.2	5.9	1.0	0.6 ± 0.2
MR02 (Δ*pntA*, Δ*sthA*)	3.6	3.4	3.6	3.4	3.5 ± 0.6
JC87 (Δ*sucC*)	8.0	6.7	6.0	4.8	2.3 ± 0.3
JC88 (Δ*pgi*, Δ*sthA*)	9.2	8.2	6.9	5.6	4.2 ± 0.7

Model parameters and constraints are described in the Materials and Methods Section. Y_{RPG} is included for comparison between simulated and experimental results.

and lactate secretion are likely the result of an elevated NADH/NAD^+ ratio causing inhibition of pyruvate dehydrogenase (Schwartz et al., 1968) and TCA cycle activity (Vemuri et al., 2006), while pyruvate-formate lyase remains inactive given the aerobic conditions (Alexeeva et al., 2000).

Transhydrogenase Deletion and Overexpression

Weckbecker and Hummel (2004) showed that plasmid-based overexpression of PntAB in *E. coli* expressing NAD^+-dependent formate dehydrogenase and $NADP^+$-dependent alcohol dehydrogenase resulted in increased rates of whole-cell production of (*R*)-phenylethanol in the presence of formate as a reductant. In contrast, Sanchez et al. (2006) showed that overexpression of SthA in *E. coli* improved the production of poly(3-hydroxybutyrate) (PHB) in an NADPH-dependent pathway. While not the physiological role of SthA, Sanchez speculated that with a sufficient NADPH drain from PHB synthesis (and therefore elevated concentrations of $NADP^+$), SthA would operate in the direction of NADPH production, and that overexpressing this enzyme would correspond to increased NADPH supply. In our study the two transhydrogenase systems PntAB and SthA were individually co-expressed with CbXR. Plasmids containing the *CbXR* gene and either the *sthA* (pPCC500) or *pntAB* (pPCC106) gene(s) were constructed. Transhydrogenase activity assays confirmed functional expression of the transhydrogenases from these plasmids (Fig. 3). The increase in transhydrogenase activity resulting from plasmid-based expression was additionally verified to be soluble for pPCC500 (~3-fold higher) and localized in membranes for pPCC106 (over 4-fold higher) (data not shown). Results for the resting cell cultures of pPCC106 and pPCC500 transformed into strain PC09 are shown in Table III. Overexpression of either transhydrogenase did not improve the Y_{RPG} in resting cells. Surprisingly, overexpression of PntAB (pPCC106) lowered the Y_{RPG} when compared to the plasmids containing only CbXR (pLOI3815) or CbXR plus SthA (pPCC500). Plasmids pPCC106 and pPCC500 were also each transformed into strain JC79 (Δ*ndh*), to test whether overexpressing either transhydrogenase could improve NADPH availability in the context of impaired NADH oxidation (and elevated NADH/NAD^+ ratio). As was the case with PC09, no improvements in Y_{RPG} were obtained (data not shown).

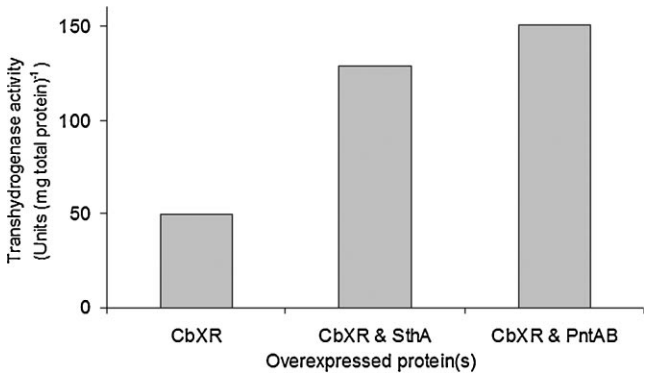

Figure 3. Transhydrogenase activities measured from lysates of *E. coli* strain PC09 harboring plasmid pLOI3815 (expressing CbXR), pPCC500 (expressing CbXR and SthA) or pPCC106 (expressing CbXR and PntAB). Activity reported as Units (mg total protein)$^{-1}$ in the lysate.

Deleting *pntA* (strain JC73), *sthA* (strain JC74), or both transhydrogenases (strain MR02) results in Y_{RPG} values of ~3.6 for all three strains. Glucose uptake and xylitol production rates were similar to that of PC09, although JC74 and MR02 produced slightly elevated amounts of acetate. Transhydrogenase assays performed on lysate fractions verified the presence of transhydrogenase activity in PC09 (Fig. 3) and decreased activity from the deletion strains were similar to those reported by Sauer et al. (2004) (not shown). While the result for JC74 may not be surprising, a reduction in Y_{RPG} relative to PC09 was expected from the *pntA* deletions, and the modeling study demonstrated the large impact that PntAB has on the theoretical maximum yield. Interestingly, the Y_{RPG} values of the *pntA* mutants are similar to the maximum theoretical yield predicted by the model (3.6). Furthermore, eliminating the PntAB reaction from other simulated strains (Δ*zwf*, Δ*pgi*, Δ*sucC*) results in theoretical maximum yield values (given in Table II) very similar to the experimentally determined values for the corresponding PC09 deletion strains given in Table III (these still carrying *pntAB*). These results suggest that transhydrogenase activity does not play a significant role in the supply of NADPH to CbXR under these assay conditions. Metabolic fluxes may be adjusted in response to altered transhydrogenase expression such that the net reducing equivalents leading to NADPH availability for xylitol production is not affected. Alternately, in vivo transhydrogenase activity in these resting cells (in strains expressing transhydrogenase) may not be significant relative to the other pathways controlling cofactor metabolism.

Strains with deletions in both *pgi* and *sthA* are unable to grow on glucose minimal medium due to the inability to oxidize excess NADPH (Sauer et al., 2004). JC88 (Δ*pgi*, Δ*sthA*) was created to determine if excess NADPH generated in this strain could be utilized for xylitol production (assuming SthA would otherwise convert the excess NADPH to NADH). Under resting cell conditions, the Y_{RPG} was similar to that observed for JC72 (~4.0), supporting the notion that SthA does not contribute to xylitol production via interconversion of reducing equivalents between cofactors.

Expression of NADH-Utilizing Xylose Reductase

Finally, we compared the resting cell Y_{RPG} obtained with NADPH-dependent CbXR expression in PC09 to that achieved when expressing the xylose reductase from *Candida tenuis* (CtXR), which has dual cofactor specificity (i.e., it can use both NADPH ($K_m \sim 4.8$ μM) and NADH ($K_m \sim 25$ μM)) (Hacker et al., 1999; Neuhauser et al., 1997)

and allows for batch culture xylitol production levels comparable to those achieved with CbXR (Cirino et al., 2006). The Y_{RPG} for PC09 harboring plasmid pPCC05 was ~4.0, which is significantly larger than the Y_{RPG} of 3.4 obtained with plasmid pLOI3815 (P-value <0.034). Thus in PC09 resting cells the net availability of reduced cofactors is not limiting the yield to 3.4. This again suggests that "excess" reducing equivalents are not readily transferred from NADH to NADPH. Transforming pPCC05 into JC72 to express CtXR in the context of the *pgi* deletion (which increased yield with CbXR) did not further improve the yield.

Discussion

Xylitol yields from strains with deletions in key central metabolism genes were compared in resting cell conditions, and compared to the theoretical maximum values. The mean Y_{RPG} values calculated for strains JC72, JC75, JC79, and JC87 are statistically different from that of PC09 at a 99% confidence level (P-values <0.002). By comparing the adjusted Y_{RPG} of PC09, JC75, and JC87, we conclude that both the TCA cycle and pentose phosphate pathway are the primary contributors of NADPH for xylitol production (in PC09). The increased Y_{RPG} with strain JC72 implies that flux at the glucose-6-phosphate node is split between the EMP and PP pathways in PC09 (as expected (Hua et al., 2003; Sauer et al., 2004; Zhao et al., 2004)). A lower experimental Y_{RPG} in strain JC87 implies that the TCA cycle is active under the employed resting cell conditions. While the TCA cycle is often considered to have very low activity under conditions of excess glucose or growth in LB medium (Cronan and Rock, 1996; Gray et al., 1966), it is possible that the added cofactor drain resulting from xylitol production and/or the *crp** mutation in PC09 contribute to the observed role of the TCA cycle in our study.

The metabolic role of transhydrogenases during *E. coli* biocatalysis has remained largely unspecified. Inferences about metabolic fluxes are readily made without considering the influence of transhydrogenases (e.g., Walton and Stewart, 2004; Zhao et al., 2004), and transhydrogenase functional roles inferred from flux analyses depend on the metabolic model and experimental conditions used (Hua et al., 2003; Sauer et al., 2004). The *pntA* and *pntA*/*sthA* mutant strains in our study (JC73 and MR02) had Y_{RPG} values similar to the maximum theoretical yields predicted by the metabolic model and similar to the Y_{RPG} for PC09. In the knockout scenarios examined, removing PntAB from the model brought maximum theoretical yields to values close to those determined experimentally. Overexpressing either transhydrogenase did not increase Y_{RPG} for the strains tested, while use of a reductase with relaxed cofactor specificity (CtXR) slightly improved the Y_{RPG} to 4.0. Thus, it seems that reducing equivalents are not readily transferred from NADH to NADPH via PntAB in this system, and the net reducing equivalents available for xylose reduction does not exceed ~4 mol per mol glucose, regardless of the specific pathways involved.

While the inability of transhydrogenase overexpression to increase yield may seem to contradict the successful implementation of PntAB overexpression by Weckbecker and Hummel (2004) and of SthA overexpression by Sanchez et al. (2006) (both using *E. coli*), it is difficult to accurately compare results between these different experimental systems. In the Weckbecker study, PntAB expression was coupled with expression of NAD^+-dependent formate dehydrogenase to increase production of (*R*)-phenylethanol from acetophenone through an NADPH-dependent reduction, with formate serving as source of reducing equivalents. While yields were not reported in that study, at most one (*R*)-phenylethanol can be produced per formate consumed, requiring complete coupling of three enzymatic reactions. In contrast, the Sanchez study involved fermentation of glucose to poly(3-hydroxybutyrate), which requires NADPH-dependent reduction of acetoacetyl-CoA. Cofactor yield per glucose cannot be assessed in the same manner as in our study, since glucose is also converted to product. In both of these examples productivity was increased upon transhydrogenase overexpression, but the relative flux through each heterologous pathway was still lower than what we report (~3.0 mmol xylitol $(g\,cdw\,h)^{-1}$ compared to ~0.4 mmol phenylethanol $(g\,cdw\,h)^{-1}$, and ~1.7 mmol 3-hydroxybutyrate $(g\,cdw\,h)^{-1}$). Perhaps as the net flux of reducing equivalents toward NADPH approaches this level, factors other than transhydrogenase activity limit further increases. The use of *crp** strains in our study (and resulting changes in gene expression) may also influence the efficacy of increasing transhydrogenase activity.

Results from this study raise important questions relating to cofactor trafficking and availability during biocatalysis in whole-cell systems. Whereas the theoretical maximum xylitol yield for strain PC09 is between 6.9 (for ATP-dependent xylose uptake) and 9.2 (for xylose-proton symport) (with growth rate and maintenance energy requirement set at 0.0092 g biomass $(g\,cdw\,h)^{-1}$ and 7.6 mmol ATP $(g\,cdw\,h)^{-1}$, respectively), the experimentally determined Y_{RPG} for non-growing cells is only 3.4. The large discrepancy between theoretical maximum and experimentally determined yield values suggests that biocatalysis is compromised by pathways competing for reducing equivalents. More than 60% of the available energy in the form of NAD(P)H resulting from glucose oxidation is "dissipated" during biotransformation (note this energy consumption is beyond the maintenance energy constraint already included in the model). While scarce, similar cofactor yield analyses with other whole-cell biocatalyst systems reveal similar results. Walton and Stewart describe expressing an NADPH-dependent short-chain dehydrogenase in *E. coli* to reduce ethyl acetoacetate under glucose-fed, non-growing conditions (Walton and Stewart, 2004). They reported the stoichiometry linking ketone reduction and glucose consumption (i.e., Y_{RPG}) to be ~2.3. Schmid analyzed NADH usage for styrene epoxidation in recombinant *E. coli* expressing styrene monooxygenase (Blank et al., 2008; Buhler et al., 2008). In aerobic continuous culture with

glucose as the growth substrate, they observed net NAD(P)H consumption that was 3.4–4.0 times higher than the amount of NADH required for styrene epoxidation, with a corresponding Y_{RPG} near one (Buhler et al., 2008). In agreement with our results, switching to resting cells improved the styrene oxide (i.e., NADH) yield to nearly three, and this yield was not significantly altered when either transhydrogenase was deleted (Blank et al., 2008).

In these examples it is unclear how the remaining reducing equivalents are dissipated. Schmid suggested that the deviations from predicted cofactor yields could be the result of increased maintenance energy requirements during biocatalysis, "energy spilling," or uncoupling of NADH oxidation from styrene oxidation by the monooxygenase (Blank et al., 2008; Buhler et al., 2008). Assuming cofactor uncoupling by xylose reductase is not a significant drain of NADPH, the remaining reducing equivalents are most likely eliminated through respiration. This suggests that under physiological conditions the PntAB and reductase reactions do not effectively compete with respiration. Decreasing respiration by reducing oxygen availability or deleting *ndh* (NADH dehydrogenase II) lowered Y_{RPG} values due to secretion of acids and fermentation products. Again, the conditions are such that transhydrogenase and reductase reactions apparently do not effectively compete for available NADH.

It is not likely that true maintenance energy requirements are the primary drain on NAD(P)H, given that resting cells in this study are unable to synthesize protein. If there is not a demand for ATP, the question becomes at what point is energy "lost"? Many scenarios can be rationalized, such as ATP hydrolysis via futile cycles, uncoupling during electron transport, dissipation of proton gradients, and significant inefficiencies in substrate transport. Addressing this issue by tracking the fate of all NAD(P)H in resting cells should provide insights toward the design of more efficient biocatalysts.

The authors thank the Keio Collection for providing the single deletion mutant strains. This work was supported by NSF grant no. BES0519516.

References

Alexeeva S, de Kort B, Sawers G, Hellingwerf KJ, de Mattos MJ. 2000. Effects of limited aeration and of the ArcAB system on intermediary pyruvate catabolism in Escherichia coli. J Bacteriol 182(17):4934–4940.

Baba T, Ara T, Hasegawa M, Takai Y, Okumura Y, Baba M, Datsenko KA, Tomita M, Wanner BL, Mori H. 2006. Construction of Escherichia coli K-12 in-frame, single-gene knockout mutants: The Keio collection. Mol Syst Biol 2:2006.0008.

Blank LM, Ebert BE, Bühler B, Schmid A. 2008. Metabolic capacity estimation of *Escherichia coli* as platform for redox biocatalysis: Constraint based modeling and experimental verification. Biotechnol Bioeng 100(6):1050–1065.

Bock A, Sawers G. 1996. Fermentation. In: Neidhardt FC, Curtiss R III, Ingraham JL, Lin ECC, Low KB, Magasanik B, Reznikoff WS, Riley M, Schaechter M, Umbarger HE, editors. *Escherichia coli* and *Salmonella*: Cellular and molecular biology. Washington, DC: ASM Press.

Buhler B, Park JB, Blank LM, Schmid A. 2008. NADH availability limits asymmetric biocatalytic epoxidation in a growing recombinant Escherichia coli strain. Appl Environ Microbiol 74(5):1436–1446.

Canonaco F, Hess TA, Heri S, Wang T, Szyperski T, Sauer U. 2001. Metabolic flux response to phosphoglucose isomerase knock-out in Escherichia coli and impact of overexpression of the soluble transhydrogenase UdhA. FEMS Microbiol Lett 204(2):247–252.

Causey TB, Zhou S, Shanmugam KT, Ingram LO. 2003. Engineering the metabolism of Escherichia coli W3110 for the conversion of sugar to redox-neutral and oxidized products: Homoacetate production. Proc Natl Acad Sci USA 100(3):825–832.

Ciotti MM, Kaplan NO. 1956. Chemistry and properties of the 3-acetylpyridine analogue of diphosphopyridine nucleotide. J Biol Chem 221(2):823–832.

Cirino PC, Chin JW, Ingram LO. 2006. Engineering Escherichia coli for xylitol production from glucose-xylose mixtures. Biotechnol Bioeng 95(6):1167–1176.

Covert MW, Palsson BO. 2002. Transcriptional regulation in constraints-based metabolic models of Escherichia coli. J Biol Chem 277(31): 28058–28064.

Cronan JE, Rock CO, editor. 1996. Tricarboxylic acid cycle and glyoxylate bypass, 2 edn. Washington, DC: ASM Press.

Datsenko KA, Wanner BL. 2000. One-step inactivation of chromosomal genes in Escherichia coli K-12 using PCR products. Proc Natl Acad Sci USA 97(12):6640–6645.

Duetz WA, van Beilen JB, Witholt B. 2001. Using proteins in their natural environment: Potential and limitations of microbial whole-cell hydroxylations in applied biocatalysis. Curr Opin Biotechnol 12(4):419–425.

Flores S, Gosset G, Flores N, de Graaf AA, Bolivar F. 2002. Analysis of carbon metabolism in Escherichia coli strains with an inactive phosphotransferase system by (13)C labeling and NMR spectroscopy. Metab Eng 4(2):124–137.

Gray CT, Wimpenny JW, Mossman MR. 1966. Regulation of metabolism in facultative bacteria. II. Effects of aerobiosis, anaerobiosis and nutrition on the formation of Krebs cycle enzymes in Escherichia coli. Biochim Biophys Acta 117(1):33–41.

Hacker B, Habenicht A, Kiess M, Mattes R. 1999. Xylose utilisation: Cloning and characterisation of the Xylose reductase from Candida tenuis. Biol Chem 380(12):1395–1403.

Haldimann A, Wanner BL. 2001. Conditional-replication, integration, excision, and retrieval plasmid-host systems for gene structure-function studies of bacteria. J Bacteriol 183(21):6384–6393.

Heller KB, Lin EC, Wilson TH. 1980. Substrate specificity and transport properties of the glycerol facilitator of Escherichia coli. J Bacteriol 144(1):274–278.

Hua Q, Yang C, Baba T, Mori H, Shimizu K. 2003. Responses of the central metabolism in Escherichia coli to phosphoglucose isomerase and glucose-6-phosphate dehydrogenase knockouts. J Bacteriol 185(24): 7053–7067.

Khankal R, Chin JW, Cirino PC. 2008. Role of xylose transporters in xylitol production from engineered Escherichia coli. J Biotechnol 134(3–4):246–252.

Miller JH. 1992. A short course in bacterial genetics: A laboratory manual and handbook for Escherichia coli and related bacteria. Cold Spring Harbor: Cold Spring Harbor Press.

Moreira dos Santos M, Raghevendran V, Kotter P, Olsson L, Nielsen J. 2004. Manipulation of malic enzyme in *Saccharomyces cerevisiae* for increasing NADPH production capacity aerobically in different cellular compartments. Metab Eng 6(4):352–363.

Neuhauser W, Haltrich D, Kulbe KD, Nidetzky B. 1997. NAD(P)H-dependent aldose reductase from the xylose-assimilating yeast Candida tenuis. Isolation, characterization and biochemical properties of the enzyme. Biochem J 326(Pt 3):683–692.

Reed JL, Vo TD, Schilling CH, Palsson BO. 2003. An expanded genome-scale model of Escherichia coli K-12 (iJR904 GSM/GPR). Genome Biol 4(9):R54.

Sambrook J, Russell DW. 2001. Molecular cloning: A laboratory manual. Cold Spring Harbor: Cold Spring Harbor Press.

Sanchez AM, Andrews J, Hussein I, Bennett GN, San KY. 2006. Effect of overexpression of a soluble pyridine nucleotide transhydrogenase

(UdhA) on the production of poly(3-hydroxybutyrate) in Escherichia coli. Biotechnol Prog 22(2):420–425.

Sauer U, Canonaco F, Heri S, Perrenoud A, Fischer E. 2004. The soluble and membrane-bound transhydrogenases UdhA and PntAB have divergent functions in NADPH metabolism of Escherichia coli. J Biol Chem 279(8):6613–6619.

Schmid A, Dordick JS, Hauer B, Kiener A, Wubbolts M, Witholt B. 2001. Industrial biocatalysis today and tomorrow. Nature 409(6817):258–268.

Schwartz ER, Old LO, Reed LJ. 1968. Regulatory properties of pyruvate dehydrogenase from Escherichia coli. Biochem Biophys Res Commun 31(3):495–500.

Tao H, Bausch C, Richmond C, Blattner FR, Conway T. 1999. Functional genomics: Expression analysis of Escherichia coli growing on minimal and rich media. J Bacteriol 181(20):6425–6440.

van der Donk WA, Zhao H. 2003. Recent developments in pyridine nucleotide regeneration. Curr Opin Biotechnol 14(4):421–426.

Varma A, Palsson BO. 1994. Stoichiometric flux balance models quantitatively predict growth and metabolic by-product secretion in wild-type Escherichia coli W3110. Appl Environ Microbiol 60(10): 3724–3731.

Vemuri GN, Altman E, Sangurdekar DP, Khodursky AB, Eiteman MA. 2006. Overflow metabolism in Escherichia coli during steady-state growth: Transcriptional regulation and effect of the redox ratio. Appl Environ Microbiol 72(5):3653–3661.

Verho R, Londesborough J, Penttila M, Richard P. 2003. Engineering redox cofactor regeneration for improved pentose fermentation in *Saccharomyces cerevisiae*. Appl Environ Microbiol 69(10):5892–5897.

Walton AZ, Stewart JD. 2004. Understanding and improving NADPH-dependent reactions by nongrowing Escherichia coli cells. Biotechnol Prog 20(2):403–411.

Weckbecker A, Hummel W. 2004. Improved synthesis of chiral alcohols with Escherichia coli cells co-expressing pyridine nucleotide transhydrogenase, NADP+-dependent alcohol dehydrogenase and NAD+-dependent formate dehydrogenase. Biotechnol Lett 26(22):1739–1744.

Zhao J, Shimizu K. 2003. Metabolic flux analysis of Escherichia coli K12 grown on 13C-labeled acetate and glucose using GC-MS and powerful flux calculation method. J Biotechnol 101(2):101–117.

Zhao J, Baba T, Mori H, Shimizu K. 2004. Global metabolic response of Escherichia coli to gnd or zwf gene-knockout, based on 13C-labeling experiments and the measurement of enzyme activities. Appl Microbiol Biotechnol 64(1):91–98.